Egypt.J.Chem. **Vol. 63**, No. 3. pp. 759-776 (2020)

Egyptian Journal of Chemistry
http://ejchem.journals.ekb.eg/

Caprylamidopropyl Betaine as a Highly Efficient eco-friendly Corrosion Inhibitor for API X120 Steel in 1 M H_2SO_4

Abd El-Aziz S. Foudaa[1*], Ali Abd El Aalb[2], Mostafa H. Sliem[2], Aboubakr M. Abdullah[3]

[1] *Chemistry Department, Faculty of Science, Mansoura University, Mansoura-35516, Egypt.*
[2] *Chemistry Department, Faculty of Science, Zagazig University, Zagazig, Egypt.*
[3] *Center for Advanced Materials, Qatar University, El-Doha, Qatar.*

CORROSION inhibition of API X120 steel in a 1M sulfuric acid solution at altered temperatures was investigated utilizing a new eco-friendly surfactant (Caprylamidopropyl Betaine (CAPB)) by Gravimetric and electrochemical test (containing potentiodynamic polarization (PP), electrochemical impedance spectroscopy (EIS). Surface characterization tests containing scanning electron microscopy (SEM), and atomic force microscopy (AFM) are utilized in the study. In addition, kinetic and thermodynamic parameters were measured and discussed. The overall results displayed that the corrosion rate of API X120 steel was significantly lowered with improving the temperature. The polarization curves lead to the CAPB inhibitor is influenced both anodic and cathodic reactions (mixed type inhibitor). Analyses of the surface topography designated an appreciable decrease in the surface roughness as the dose of the inhibitor in the solution improved. Energy-dispersive X-ray and X-ray photoelectron spectroscopy revealed the presence of adsorbed nitrogen atoms on the API X 120 steel surfaces. This work provides a promising eco-friendly inhibitor for mitigating the corrosion of API X120 steel in highly acidic brine environments.

Keywords: API X120 steel; Caprylamidopropyl Betaine; Quantum Calculations.

Introduction

One of the important mineral acids that is widely used in many applications, including well acidizing, water treatment, chemical cleaning, and acid pickling, are hydrochloric and sulfuric acid [1-4]. The selection of cost-effective materials to handle this acid requires extreme care and detailed engineering. The presence of certain impurities, such as ferric salts, cupric salts, and chlorine, in the acid and/or a high level of aeration amplifies the oxidizing power of the solution, leading to accelerated corrosion damage [5-6]. In the oil and gas industry, the exposure of materials to acidic environments is more common and frequent than to neutral or alkaline environments [7-10]. This necessitates exploring options and efficient techniques to mitigate and control the corrosion of iron and its alloys, as they constitute a large fraction of the metallic materials that are exposed to acidic media. Corrosion inhibitors are widely utilized to mitigate corrosion risks. Unfortunately, some of the effective corrosion inhibitors used to mitigate corrosion are highly toxic. Increased environmental awareness and the development of regulations have imposed restrictions on the use of such inhibitors. Additionally, the safe disposal of corrosion inhibitors after use or the treatment of contaminated streams is critical and usually defined as a step in all chemical treatment programs, which adds to the corrosion control cost. The environmental and safety concerns related to corrosion inhibition processes have encouraged researchers to explore alternatives that are eco-friendly and offer acceptable inhibition efficiency, especially in acidizing treatment processes, which cost in addition to chemical treatment applications, a direct expenses close to 8 billion USD per year

*Corresponding author e-mail: asfouda@hotmail.com, Fax:+2 050 2202264, Tel: +2 050 2365730 Tel:+2 050 2365730, Fax: +2 050 2202264
Received 13/6/2019; Accepted 8/7/2019
DOI: 10.21608/ejchem.2019.13652.1844

[11]. Therefore, focus on natural and nature-based products is increased to produce so-called "green inhibitors" [12-15]. However, the severe acidic and high-temperature environments during drilling and stimulation processes in the oil and gas wells limit the full utilization of such green corrosion inhibitors. The development of green corrosion inhibitors that resist severe acidic corrosive environments and control the corrosion of API X120 steel [16-17], particularly in well acidizing, is highly desired. A number of researches reduce the steel corrosion in acidic media by means of the surfactants [18-19]. On the other hand, caprylamidopropyl Betaine has been utilized as a stabilizer for oil water emulsions due to its zwitterionic ability with the aid of silica nanoparticles [20]. Moreover, caprylamidopropyl Betaine gives a tremendous synergistic interaction with colloidal silica leading to a newly viscous and stable generation of CO_2-water foams [21].

In this work, Caprylamidopropyl Betaine (CAPB) is tested as an inexpensive, highly efficient, and eco-friendly corrosion inhibitor for API X120 steel in 1 M H_2SO_4 solution at ambient and elevated temperatures using various electrochemical techniques. In addition, several surface characterization methods are used. Furthermore, the kinetic and thermodynamic parameters are measured and/or calculated. A geometry optimization of CAPB is also performed and the electronic absorption spectra are calculated using the time-dependent density functional theory. Furthermore, frequency calculations are also performed on the optimized geometry.

Experimental Technique

Materials and solutions

The chemical composition of the API X120 steel used in this work, shown in Table 1, was elementally analyzed using an optical emission spectrometer (ARL 3460, Thermo Fisher Scientific, and Waltham, MA, USA).

Coupons of equal size (1.5 × 1.5 × 0.5 cm^3) were cold-cut from API X120 steel plate. They were polished using SiC emery papers from 250 down to 4000 grit, washed with ethanol for 10 min in an ultrasonic bath, then degreased with acetone for 1 min, followed by rinsing with ethanol. They were then rinsed again with deionized water and finally dried using air. The corrosive acidic solution that was used in this work was prepared by diluting analytical H_2SO_4, which has a dose of 98%, using distilled water to produce a 1 M H_2SO_4 solution. CAPB, the chemical structure of which is shown in Fig. 1, was used as a green corrosion inhibitor and was obtained from Shanghai Dejun Technology Co., Ltd, Shanghai, China.

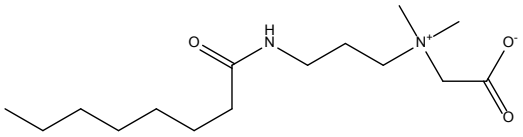

Fig. 1. CAPB chemical structure (1-Propanaminium, N-(carboxymethyl)-N, N-dimethyl-3-[(1-oxooctyl) amino], Molecular formula $C_{17}H_{34}N_2O_3$, Molecular weight = 314.47.

Weight loss (WL) measurements

WL measurements were obtained from API X120 steel sheets with dimensions 2.5 x 2.0 x 0.2 cm. The sheets were mechanically cleaned first with different grades of emery papers (320, 600 & 1000), washed with ethanol, then rinsed in deionized water and dried. The prepared metal sheets were suspended freely in 200 ml glass beakers containing 100 ml of the corrosive solutions (1 M H_2SO_4 and 1 M H_2SO_4 with various doses of CAPB) at 25°C. The specimens were removed after 3 h and treated following the method described in ASTM designation G1-90 [22]. The corrosion rate (mpy) was computed based on Eq. 1 [23-24]:

$$\text{Corrosion rate (mpy)} = (534\ W)/(\rho\ A\ t) \quad (1)$$

Where w is the WL in mg, $\boldsymbol{\rho}$ is the API X120 steel density in g/cm^3, A is the surface area of the sample in square centimeters, and t is the time of the test in hours.

The (IE %) and the surface coverage θ of the surfactant used for the corrosion of API X120 steel was calculated as follows:

TABLE 1. Elemental composition analysis for API X120 steel.

Element	C	Mn	Si	Ni	Mo	S	V	Cr	Fe
Weight %	0.103	0.39	0.101	0.017	0.001	0.04	0.025	0.035	Balance

$$IE\ \% = \theta \times 100 = ((W^{o}-W))/W \times 100 \quad (2)$$

Where w^o and w are the average WL values without and with adding the surfactant, respectively.

Electrochemical measurements

A 250 ml double-jacketed three-electrode corrosion cell was used, in which a graphite rod and an API X120 steel coupon with an area of 0.5 cm^2 exposed to the corrosive solution were the counter and working electrodes, respectively. The reference electrode was a saturated calomel electrode (SCE). To minimize the *IR* drop, the SCE was used with a Luggin capillary. A Julabo F12 thermostat water circulator (Seelbach, Germany) was used to control the temperature between 20 and 80°C. A thermometer was used to monitor the temperature of the electrolyte before and during the experiments. A Reference 300 GAMRY Potentiostat (Warminster, PA, USA) was used to perform the electrochemical measurements. The GAMRY measurement software packages include EIS300 for EIS and DC105 for corrosion analysis. The open-circuit potential (E_{OCP}) of the working electrode was stabilized before any electrochemical testing by placing it in the solution for 30 min. The EIS measurements were performed within a frequency range of 0.1 to 10^5Hz, with a 10 mV AC peak-to-peak amplitude. Tafel polarization curves were recorded by scanning the potential between −250 and +250 mV with respect to E_{OCP} in the more noble direction. The sweep rate was always 0.3 mVs^{-1}. Four different doses of the corrosion inhibitor were used: 25, 50, 70, and 100 μmol L^{-1}.

Surface analysis

Surface analysis plays an important role in characterizing the surface morphology and studying the effect of the inhibitor and its interaction with the substrate. Immersion tests were conducted to quantify the effect of the corrosive acidic medium on the API X120 steel electrode and to study the surface topography before and after the addition of the CAPB inhibitor. Three API X120 steel specimens were ground to a 4000 grit and then polished to a mirror-like finish using alumina suspensions of different particle size. The coupons were immersed in a 1 M H_2SO_4 solution without the addition of a corrosion inhibitor for 24 h at 25 °C. The same procedure was repeated, but with the addition of 100 μmol L^{-1} of the CAPB corrosion inhibitor. The morphology of the samples after immersion in the absence of the CAPB inhibitor was examined and compared to that of samples exposed to an inhibited solution using a high field emission scanning electron microscope (HFESEM) (FEI NOVA NANOSEM 450, Hillsporo, OR, USA), typically operated with an acceleration voltage of 20kV coupled with an EDX unit. The adsorbed inhibitor on the API X120 steel was analyzed using XPS (AXIX Ultra DLD, Kratos, UK), employing a monochromatic Al Kα X-ray source as the incident radiation source, and the binding energy of C 1s (284.6 eV) was utilized as a reference. AFM analyses (MFP-3D, Asylum Research, Goleta, CA, USA) were performed using a silicon tip of radius 10 nm, with a resonance frequency of 70 kHz and a spring constant of 2 Nm^{-1} in the non-contact tapping mode in air.

Results and Discussion

Weight loss (WL) measurements

To evaluate the influence of the CAPB doses on inhibition efficiency, WL measurements were done on API X120 steel specimens for various immersion times at room temperature. The results could be attributed to the ability of CAPB to be adsorbed in the API X120 steel surface because of the increased immersion time. However, the values of corrosion parameters by WL could be different in comparison with those obtained electrochemically while taking into consideration the effect of the experimental conditions.

From Fig. 2, the order of protection effectiveness of the tested corrosion inhibitor increases with increasing the dose of CAPB. This may be because of the presence of amide group in the structure, which makes the formation of a π bond resulting from overlap of 3d electrons from an iron atom to the lone pair of electrons from the nitrogen and oxygen atoms possible [25-26], thus improving the inhibition protection of the molecule on the metal surface. Indeed, the higher molecular weight of CAPB changes the inhibition efficiency. Therefore, in the presence of CAPB, the corrosion rate (CR) is an indicator for the number of free corrosion sites remaining after effectively blocking of the other sites by inhibitor adsorption [27-28]. Assuming that corrosion occurs only at the free sites while neglecting the CR of the covered sites, the (%IE) can be calculated by Equation 1 using the degree of surface coverage. Table 2 shows the results for (%IE) at different doses of CAPB on API X120 steel after various immersion times at room temperature. It is clear that the CR decreases in the presence of CAPB.

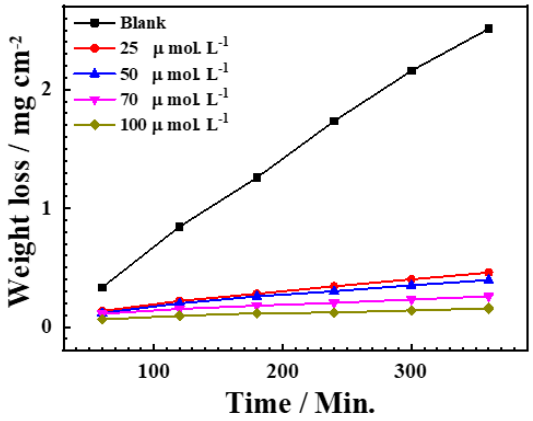

Fig. 2. WL-time curves of API X120 steel in 1 M H_2SO_4 in the absence and the presence of 20, 50, 70, and 100 µmol L^{-1} of CAPB at 25 °C.

TABLE 2. IE % of CAPB surfactant on API X120 steel dissolution in 1 M H_2SO_4 after different exposure times at 25 °C

Conc.,	Inhibition efficiency (%IE)					
µmol L^{-1}	1	2	3	4	5	6
25	59.5	74.0	77.7	80.2	81.4	81.7
50	64.7	76.4	79.5	82.6	83.7	48.2
70	66.7	81.9	85.6	88.2	89.2	89.7
100	80.8	88.8	90.8	92.9	93.5	93.8

Potentiodynamic Polarization (PP) Studies

Figure 3 illustrates the PP curves of API X120 steel in 1 M H_2SO_4 in the absence and presence of the CAPB corrosion inhibitor at various doses and temperatures. The corrosion potential (E_{corr}), corrosion current density (i_{corr}), cathodic Tafel slope ($_c$), and anodic Tafel slope ($_a$) are calculated and presented in Table 3.

In addition, the (*IE* %) and θ in Table 3 are calculated using Eqs. (5) and (6), respectively [29].

$$IE\% = ((i_1 - i_2)/i_1) \times 100 \quad (5)$$

$$\Theta = (IE\%)/(100) \quad (6)$$

Where i_1 and i_2 are the corrosion currents in the absence and presence of the corrosion inhibitor, respectively. Furthermore, the Stern–Geary equation, Eq.(7), is utilized to calculate the polarization resistance [30-31]:

$$R_p = (\beta_c \beta_a)/(2.303\ i_{corr}\ (\beta_c + \beta_a)) \quad (7)$$

Table 3 reveals the direct relation between the inhibitor dose and the reduction in the corrosion rate. A gradual increase in the IE% was noticed as the inhibitor doses increases. A maximum of IE% (98%) is attained at 20 °C with an inhibitor dose of 100 µmol L^{-1}. Elevating the temperature to 50°C decreases the *IE*% to 69%. It is also lucid that the R_p values are inversely proportional to the corrosion current density based on ohm's law. The parallel anodic and cathodic Tafel lines and their slopes suggest that the cathodic reaction is primarily activation-controlled and there is no change in the mechanism of the corrosion with and without inhibitor. It is reported that the shift in the E_{corr} by 85 mV, in the more or less noble directions after the addition of an inhibitor, classifies it as an anodic or cathodic inhibitor, respectively [32]. Otherwise, the inhibitor is considered of the mixed type category, i.e., it suppresses both reactions. As the overall shift in E_{corr} after the addition of the corrosion inhibitor is insignificant, i.e., less than 85 mV, CAPB is considered a mixed-type inhibitor [30, 33-34]. Figure 3 shows bends in the anodic polarization curves at high inhibitor doses, at all temperatures except for 50°C. This can be attributed to the alteration of the surface area covered with the corrosion inhibitor, due to the rearrangement of the adsorbed inhibitor molecules on the electrode surface and/or the destabilization of the thin protective layer formed over the substrate. Additionally, a change in the adsorption or desorption rate of the inhibitor molecules or a local change in the inhibition mechanism for the anodic reaction [35] could be reasons for the appearance of these bends.

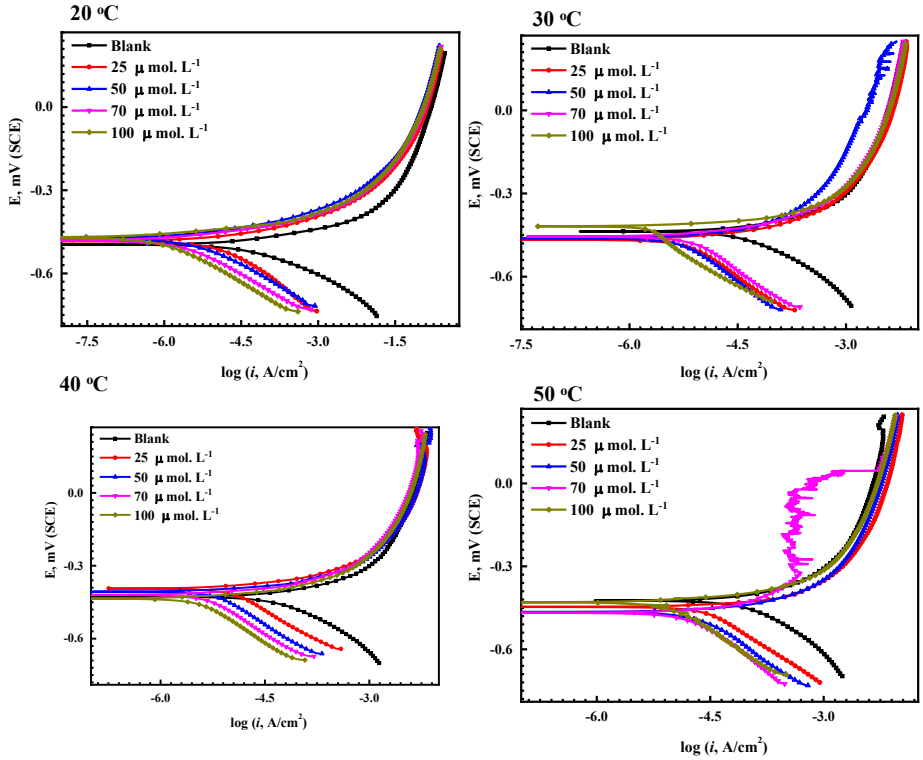

Fig. 3. PP curves of API X120 steel in a 1 M H_2SO_4 solution, before and after the addition of different doses of CAPB at a) 20°C, b) 30°C, c) 40°C, and d) 50°C.

TABLE 3.PP parameters for API X120 steel in a 1 M H_2SO_4 solution in the absence and presence of the CAPB corrosion inhibitor at various temperatures

Temp. °C	C_{inh} µmol L^{-1}	$-\beta_c$ mV dec^{-1}	β_a mV dec^{-1}	R_p Ω cm^2	E_{corr} mV vs SCE	i_{corr} µA cm^{-2}	*CR*, mpy	*θ*	*IE%*
20	----	319	162	237.6	-391.5	195.68	221.9	----	----
	25	863	116	735.2	-410.7	60.06	68.1	0.693	69.362
	50	175	193	1503	-381.2	26.56	30.1	0.864	86.4
	70	168	169	2487	-415.1	14.72	16.7	0.924	92.47693
	100	151	135	7914	-386.7	3.91	4.4	0.980	98.0
30	----	300	242	216.3	-435.1	268.97	305.1	----	----
	25	277	212	466	-415.1	111.71	126.8	0.585	58.55012
	50	254	206	1048	-395.5	47.15	53.5	0.825	82.5
	70	243	190	1442	-391.1	32.08	36.4	0.881	88.16998
	100	240	176	4656	-373.8	9.48	10.8	0.965	96.5
40	----	343	265	191.4	-432.7	339.03	384.5	----	----
	25	328	216	317.1	-393.3	178.58	202.5	0.473	47.32487
	50	323	207	505.1	-397.6	108.59	123.2	0.680	68.06828
	70	317	197	755.8	-386.7	69.89	79.2	0.794	79.4
	100	309	190	1402	-379.1	36.46	41.4	0.892	89.24401
50	----	347	278	168.1	-434.8	399.39	453.0	----	----
	25	368	227	217.0	-426.0	280.95	318.6	0.297	29.7
	50	343	213	265.1	-421.7	215.27	244.2	0.461	46.10141
	70	331	208	341.5	-417.3	162.51	184.3	0.593	59.3
	100	320	199	467.4	-450.1	114.02	129.3	0.714	71.4

EIS studies

EIS is widely employed to provide useful information about the kinetic and mechanisms of electrochemical systems [36-38]. The typical equivalent electrical circuit that is used to analyze all the measured EIS data in this study is consisted of a charge transfer resistance (R_{ct}), solution resistance (R_s), and constant phase element (CPE) used to describe the non-ideal behavior of the double layer, which is mainly attributed to non-uniform surface coverage and/or surface roughness.

The impedance of the CPE is analyzed using Eq. 8 [39]:

$$ZQ = [Y0\,(jw)n]-1 \quad (8)$$

Where Z_Q represents the CPE impedance ($\Omega\ cm^{-2}$), Y_0 is the CPE constant, ω is the frequency in rad s^{-1}, and the values of n range between 0 and 1 and define the divergence from capacitance linearity. When $n = 1$, the CPE constant Y_0 is equivalent to that of an ideal capacitor. When $n = 0$, Y_0 is equivalent to that of a resistor. The measured (dotted lines) and fitted (solid lines) impedance spectra shown in Fig. 4 are for API X120 steel in 1 M H_2SO_4 in the absence of the inhibitor at 20, 30, 40, and 50 °C. It is clear that the semicircles decrease in size as the temperature incrementally increases from 20 to 50°C. Figure 4 shows the Nyquist plots, of API X120 steel in a1 M H_2SO_4 solution in the presence of various doses of the CAPB corrosion inhibitor at (a) 20, (b) 30, (c) 40, and (d) 50 °C. The low impedance modulus (Z) increases in line with the increase in the inhibition dose, which is an indication of increased adsorption of the inhibitor molecules on the metallic substrate. Table 4 shows the electrochemical parameters obtained from fitting the measured EIS data using the equivalent circuit. The inhibition efficiency ($IE\%$) is calculated using Eq. (9) [40-41]:

$$IE\% = ((R_{ct2}-R_{ct1})/R_{ct1}) \times 100 \quad (9)$$

Where R_{ct1} and R_{ct2} represent the charge transfer resistance before and after the addition of the CAPB corrosion inhibitor, respectively. The surface coverage (θ) of the inhibitor is calculated using Equation (5). The charge transfer resistance (R_{ct}) and the constant phase parameters (Y_0 and n) are used to calculate the metal solution interface double layer capacitance (C_{dl}) using Eq. (10) [42]:

$$C_{dl} = (Y_0 R_{ct}^{1-n})^{1/n} \quad (10)$$

Table 4 reveals that R_{ct}, increases with the increase in the inhibitor dose. This increase in the R_{ct} is attributed to the adsorbed molecules of CAPB on the API X120 steel forming a barrier film, which hinders the H_2SO_4 solution from reaching the metal surface. On the contrary, the double layer capacitance was gradually decreased as the inhibitor dose increases.

The decrease in the double layer capacitance is primarily caused by (i) the decrease in the dielectric constant ($\mathcal{E}$) due to the replacement of water species by inhibitor molecules and (ii) the increase in the double layer thickness (δ) caused by the adsorption of the inhibitor on the surface, as indicated by the Helmholtz equation [43]:

$$C_{dl} = (\mathcal{E}\,\mathcal{E}_0 A)/\delta \quad (11)$$

Where A represents the cross-sectional area of the electrode and $\mathcal{E}_0$ and $\mathcal{E}$ represent the dielectric constants of air and water, respectively. As the ($IE\%$) is directly proportional to R_{ct} in the presence of the inhibitor, it also increases as the dose of the inhibitor increases and decreases as the temperature is raised, as seen in Table 4. It is important to note that the value of n is the highest in the absence of CAPB at any temperature and decreases as the inhibitor dose increases at a given temperature. In addition, the higher the temperature is, the higher is the value of n at any dose of CAPB. The values of n (approaching unity) indicate that the *CPE* is getting closer to the ideal capacitor behavior. This is primarily attributed to the inhomogeneity of the inhibitor surface coverage as the inhibitor dose increases. It is noteworthy that the EIS measurements summarized in Table 4 are consistent with the Tafel analyses shown in Table 3.

Adsorption Isotherm and Thermodynamic Calculations

The adsorption of an organic inhibitor on a metal surface in an aqueous solution is usually considered as a quasi-substitution process in which inhibitor molecules replace a number of solvent atoms, e.g., water, in a fixed size ratio. Adsorption isotherms are used extensively to illustrate and characterize the interaction between the applied corrosion inhibitor and the metallic substrate.

To identify the isotherm that best describes the adsorption of the inhibitor on the API X120 steel surface, a number of isotherms are evaluated, including Langmuir, Frumkin, and Temkin. Langmuir is found to be the best isotherm by far that fits the experimental data collected for the tested

corrosion inhibitor. It means that the adsorption of the CAPB molecule would be described by two main types of interaction: physical adsorption and chemisorption, that are influenced by the nature and charge of the metal, the molecular structure of the inhibitor and the type of electrolyte [44-45]. The Langmuir isotherm relates C_{inh} and Θas follows [46-47]:

$$C_{inh}/\Theta=1/K_{ads}+C_{inh} \quad (12)$$

Where C_{inh} is the dose of the inhibitor, Θ is the extent of surface coverage, and K_{ads} is the adsorption equilibrium constant, which can be obtained from the intercept of the plots shown in Fig. 5. Figure 5 shows the relation between C_{inh}/Θ and C_{inh} at various temperatures. The standard Gibbs free energy change of adsorption (ΔG^{o}_{ads}) can be readily obtained using Equation (13) after getting the constants of adsorption (K_{ads}) at different temperatures from the (C_{inh}/Θ)-intercepts of the plots in Fig. 5 [48].

$$K_{ads}=1/55.5\ e^{(-(\Delta Go\_ads)/RT)} \quad (13)$$

Where R is the universal gas constant, T is the temperature in Kelvin, and the value of 55.5 represents the dose of water molecules in the solution in mol L^{-1} [31].

By plotting ln K_{ads} versus T^{-1}, as shown in Fig. 6, a straight line is obtained, which follows the van't Hoff Eq. [49]:

$$\ln K\_ads=(-\Delta H^{0}_{ad})/RT+(\Delta S^{0}_{ads})/R \quad (14)$$

Where ΔS^{0}_{ads} and ΔH^{0}_{ads} are the entropy change and standard enthalpy of adsorption, respectively. By determining ΔH^{0}_{ads} from the slope of Equation (14), the entropy change of adsorption can be obtained from the interceipt. Moreover, ΔS^{0}_{ads} is calculated utilizing from Eq. (15) [50].

$$\Delta G^{0}_{ads} = \Delta H^{0}_{ads} - T\,\Delta S^{0}_{ads} \quad (15)$$

Table 5 lists the values of the thermodynamic parameters ΔH^{0}_{ads}, ΔS^{0}_{ads}, K_{ads}, and ΔG^{o}_{ads}, for the adsorption of the CAPB corrosion inhibitor at the API X120 steel surface in 1 M H_2SO_4.

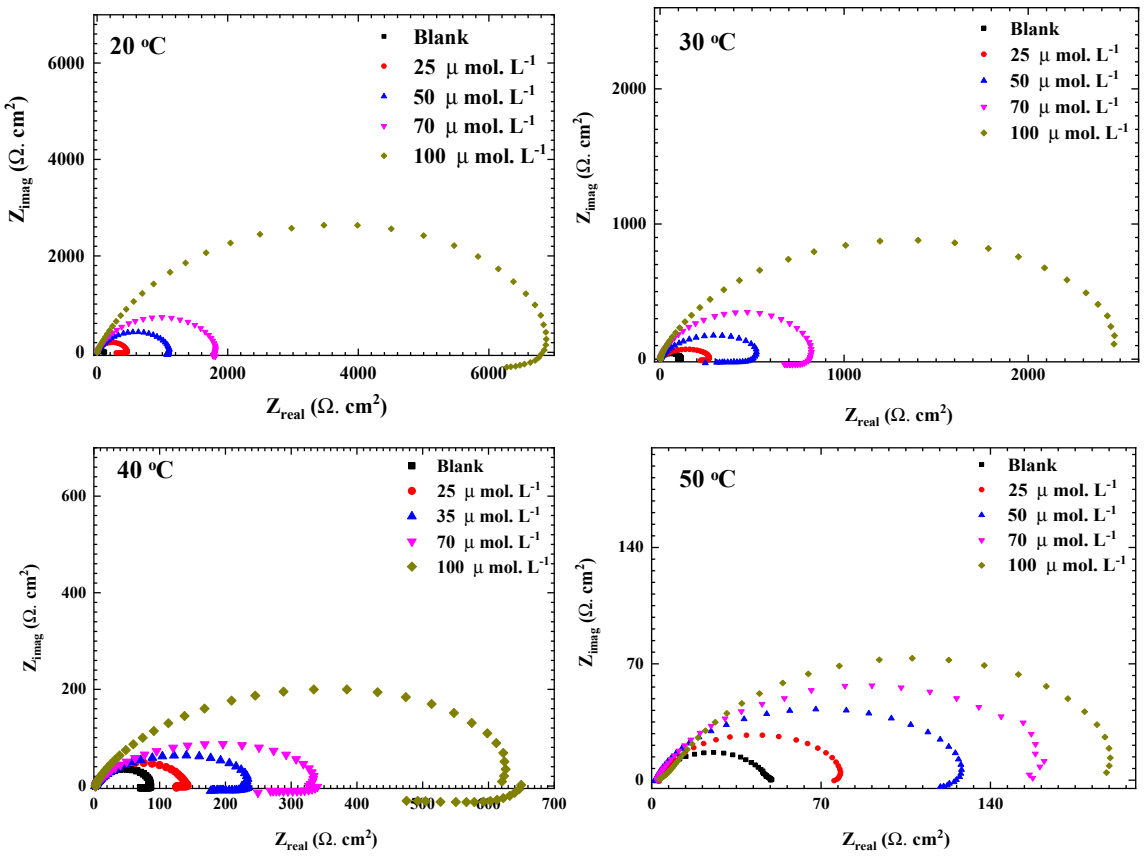

Fig. 4. EIS Nyquist plots for API X120 steel in 1 M H_2SO_4 in the presence of different doses of CAPB corrosion inhibitor at (a) 20°C, (b) 30°C, (c) 40°C, (d) 50°C

TABLE 4. EIS corrosion parameters for API X120 steel in a 1 M H_2SO_4 solution at various temperatures before and after addition of CAPB inhibitor.

T (°C)	C_{inh}, µmol L^{-1}	R_{ct}, Ω cm^2	*CPE*		C_{dl}, µF	*Θ*	*IE%*
			$Y_0 \times 10^{-6}$ $s^n\Omega^{-1}$ cm^{-2}	*n*			
20	Blank	137.2	622.1	0.894	465.16	----	----
	25	414.4	490.9	0.908	418.05	0.668	66.8
	50	912.4	454.0	0.876	400.86	0.849	84.9
	70	1665	382.4	0.976	378.42	0.917	91.7
	100	7078	351.4	0.981	357.58	0.980	98.0
30	Blank	107.6	647.1	0.918	510.23	----	----
	25	231.9	508.8	0.982	489.33	0.536	53.6
	50	511.4	467.1	0.968	445.75	0.790	79.0
	70	731.9	401.5	0.988	396.03	0.853	85.3
	100	2512	362.2	0.967	361.09	0.957	95.7
40	Blank	81.23	702.0	0.907	524.64	----	----
	25	143.6	657.9	0.897	503.07	0.434	43.4
	50	235.0	634.0	0.879	488.26	0.654	65.4
	70	339.7	599.4	0.819	422.35	0.761	76.1
	100	628.4	578.0	0.718	388.38	0.871	87.1
50	Blank	52.43	781.9	0.901	552.35	----	----
	25	78.09	711.5	0.902	520.11	0.328	32.8
	50	125.2	687.7	0.887	504.74	0.581	58.1
	70	160.9	661.4	0.851	447.69	0.673	67.3
	100	188.4	637.6	0.827	410.14	0.722	72.2

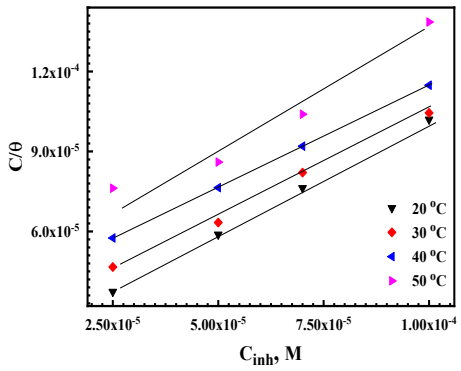

Fig. 5. Langmuir adsorption plots at various temperatures for API X120 steel in 1 M H_2SO_4

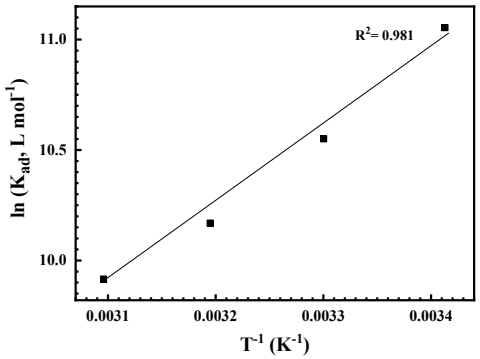

Fig. 6. Relationship between ln K_{ads} and T^{-1} for the CAPB inhibitor at the API X120 steel surface in a 1 M H_2SO_4 solution.

TABLE 5. Thermodynamic parameters derived and calculated from the Langmuir adsorption isotherm at various temperatures shown in Figure 6.

Temperature, K	K_{ads}, L mole^{-1}	$-\Delta G^0_{ads}$, kJ mol^{-1}	$-\Delta H^0_{ads}$, kJ mol^{-1}	ΔS^0_{ads}, J mol^{-1} K^{-1}
293	2020	33.9	30.0	13.41
303	2610	35.7		18.89
313	3820	37.9		25.22
323	6320	40.5		32.37

The positive values of the entropy change of adsorption ΔS^0_{ads} indicate that the adsorption of the corrosion inhibitor on the API X 120 steel surfaces is accompanied by an increase in the system entropy. This is attributed to the exothermic nature of the adsorption process, as seen from the negative value of the standard enthalpy of adsorption ΔH^0_{ads}. The high values for the constant of adsorption (K_{ads}), particularly at 25°C, for the studied CAPB inhibitor indicates strong adsorption on the API X120 steel substrate. Large K_{ads} values suggest a strong adsorption tendency and hence a better inhibition performance. This is explained by the presence of π-electrons in the inhibitor's inherent molecular structure. The negative values of ΔG^0_{ads} are aligned with the spontaneity of the inhibitor adsorption on the metal surface. The values of ΔG^0_{ads} are usually interpreted in relation to the nature of the adsorption process: whether it is physisorption or chemisorption. Generally, if the values of ΔG^0_{ads} are more than −20 kJ mol^{-1}, then the physisorption mechanism is favored, whereas if the values of ΔG^0_{ads} are −40 kJ mol^{-1} or lower, then the adsorption process is chemisorption, i.e., it involves charge sharing or transfer from the inhibitor's molecules to the protected surface to form coordination bonds. As seen in Table 5, the obtained ΔG^0_{ads} for the inhibition of API X120 steel corrosion in a 1 M H_2SO_4 solution using the CAPB inhibitor ranges from −33.9 to −40.5 kJ mol^{-1}, which is between −20 and −40 kJ mol^{-1}.Thus, the process cannot be classified as chemisorption or physisorption. Rather, it is a mixed of chemisorption and physisorption.

Effect of thermal activation on Corrosion Rate

The inhibition mechanism and efficiency are directly influenced by the apparent activation energy (E_a). The rate of most chemical reactions tends to increase as the temperature increases. It is essential to calculate the activation energy in the presence and absence of the CAPB inhibitor at various temperatures. The effect of temperature on the corrosion rate of API X120 steel can be evaluated using the Arrhenius equation:

$$\log CR = \log A - E_a/(2.303\,RT) \quad (16)$$

Where CR is the corrosion rate expressed in terms of i_{corr} at a specific temperature (T), (E_a) is the activation energy, R is the universal gas constant, and A is the Arrhenius constant, which is affected by the metal type and electrolyte composition. The Arrhenius plots of the API X120 steel logarithmic current density (log i) versus 1/T before and after the addition of the corrosion inhibitor are given in Fig. 7, with a linear regression constant that is close to unity.

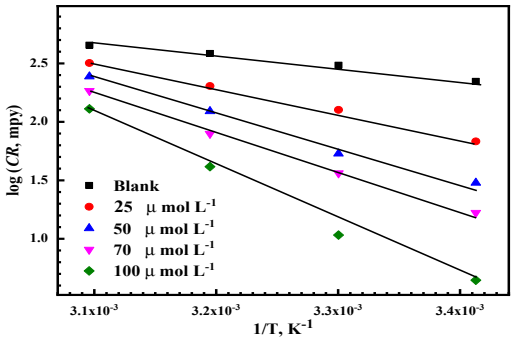

Fig. 7. Arrhenius plots for the corrosion current densities (log i) versus 1/*T* for API X120 steel at various doses of the CAPB in 1 M H_2SO_4

The apparent E_a calculated from the slopes of the plots in Fig. 7 are listed in Table 6. It is apparent from the table that E_a increases as the inhibitor dose is increased. The higher value of E_a is attributed to the formation of a barrier film of the inhibitor molecules at the surface of the API X120 steel. The entropy of activation (ΔS^*) and the enthalpy of activation (ΔH^*) due to the dissolution of API X120 steel in 1 M H_2SO_4 are calculated using the transition state theory Eq. [35]:

$$CR = RT/Nh \exp^{((\Delta S^*)/(R))} \exp^{((-\Delta H^*)/RT)} \quad (17)$$

Where h is Planck's constant, R is the universal gas constant (8.314 J mol^{-1} K^{-1}), N is Avogadro's number, and ΔH^* and ΔS^* are the enthalpy and entropy of activation, respectively.

TABLE 6. Activation energy (E^*_a), regression coefficient (R^2), enthalpy of activation (ΔH^*), and entropy of activation (ΔS^*) for API X120 steel in 1 M H_2SO_4 in the absence and presence of various doses of the CAPB inhibitor.

Conc. µmol L^{-1}	$-E^*_a$ kJ mol^{-1}	R^2	$-\Delta H^*$ kJ mol^{-1}	$-\Delta S^*$ J mol^{-1} K^{-1}
Blank	18.7	0.95	16.1	144.4
25	22.5	0.97	20.0	141.0
50	24.2	0.97	21.6	138.3
70	29.6	0.97	27.0	124.9
100	32.5	0.98	29.9	119.2

As shown in Fig. 8, straight lines are obtained by plotting log i/T versus $1/T$ at various doses of the CAPB inhibitor. The slope of $(\Delta H^*/2.303R)$ and the intercept of $[\log (R/Nh) + (\Delta S^*/2.303R)]$ are used to calculate ΔH^* and ΔS^*, respectively. The average difference between E_a and ΔH^* is approximately 2.6 kJ mol^{-1} for each test, which is almost the value of RT (2.63 kJ mol^{-1}) [51-52]. This indicates that the dissolution of API X120 steel in this environment is a unimolecular reaction.

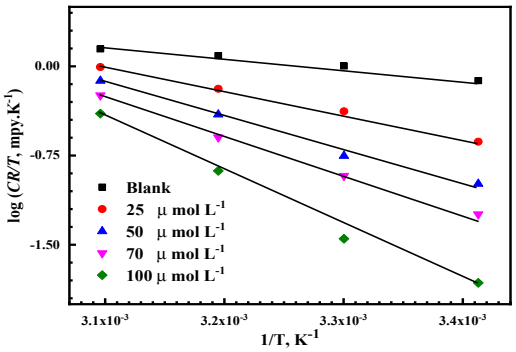

Fig. 8. Transition-state plots of log i_{corr} /T versus 1/T for API X120 steel in 1 M H_2SO_4 in the absence and presence of various doses of the CAPB.

Surface topography and characterization

Scanning electron microscopy (SEM) analysis

Figure 9 depicts SEM micrographs that revealed the morphology of the API X120 steel surface after immersion for 24 h in (A) free sample of API X120 steel, (B) in 1 M H_2SO_4 solution only and (C) in 1 M H_2SO_4 and in the presence of the CAPB inhibitor at a dose of 100 µmol L^{-1}. The testing temperature is maintained at 20°C during all experiments. Figure 9B shows that the examined surface is heavily corroded, but Fig.9C the surface was smoother due to the formation of adsorbed film from the inhibitor.

XPS analysis

The XPS survey of the adsorbed inhibitor and the high-resolution XPS analysis of C, O, and N are shown in Fig. 10 for steel after immersion in a 1 M H_2SO_4 solution inhibited by 100 µmol L^{-1} of the CAPB at 25°C. The high-resolution XPS spectrum for C 1*s* is deconvoluted into three different peaks. The first peak at 284.7eV is related to the C-C of the adsorbed inhibitor [53]. In addition, a peak at 288.1 eV is credited to the existence of carbonyl groups (-C=O) [54-55] and a third at 286.2 eV could be ascribed to the C-N of the adsorbed inhibitor on the protected metal surface [56]. The deconvolution of the O 1*s* spectrum yields three peaks. The first at 529.6 eV is related to O^{2-}, which is mainly is associated with oxygen atoms bonded to the ferric oxides (Fe_2O_3) [57]. The second one at 531.5 eV is attributed to the OH^- of hydrous iron oxides (FeOOH) [58]. The third peak observed at 533.5 eV could be ascribed to the existence of oxygen in the adsorbed water [59]. On the contrary, the deconvolution of the N 1*s* spectrum peak results in two peaks around 399.8 and 402.3eV, which are mainly attributed to the N atoms bonded to the steel surface (N-Fe) and to the protonated nitrogen atoms, respectively [60]. XPS confirms the presence of the adsorbed CAPB inhibitor on the metal surface.

Atomic force microscopy (AFM) analysis

The surface roughness and topography are analyzed using AFM. Figure 11 shows three-dimensional images of two API X120 steel samples that had been ground using SiC to 4000 grit and immersed in 1 M H_2SO_4 for 24 h with and without the addition of 100 µmol L^{-1} of the CAPB corrosion inhibitor. The average roughness of API X120 steel surface in the absence and presence of CAPB in 1 M H_2SO_4 is approximately 43.4 and 16.4 nm, respectively. The appreciable decrease in the surface roughness after the addition of inhibitor demonstrates the good inhibition performance of the CAPB corrosion inhibitor in 1 M H_2SO_4.

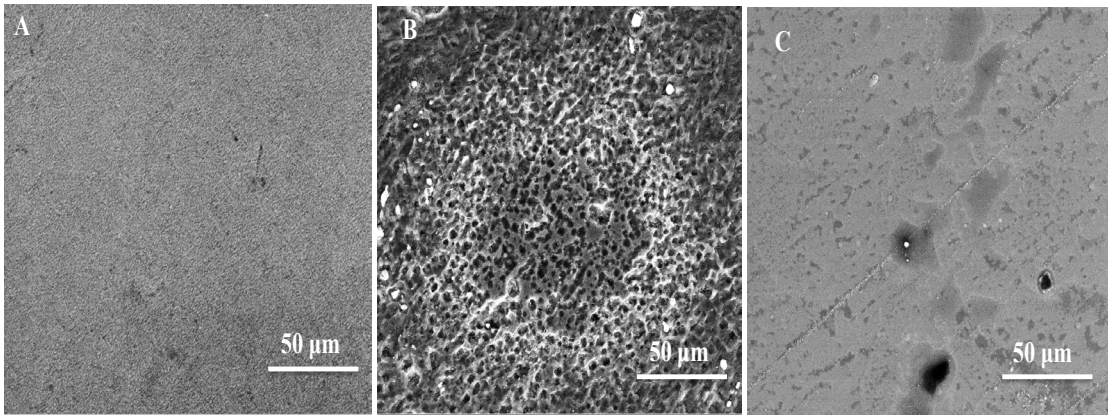

Fig. 9. SEM surface analysis micrograph for API X120 steel immersed in 1 M H_2SO_4 for 24 h in the absence and presence of 100 µmol L^{-1} of the CAPB inhibitor at 20°C

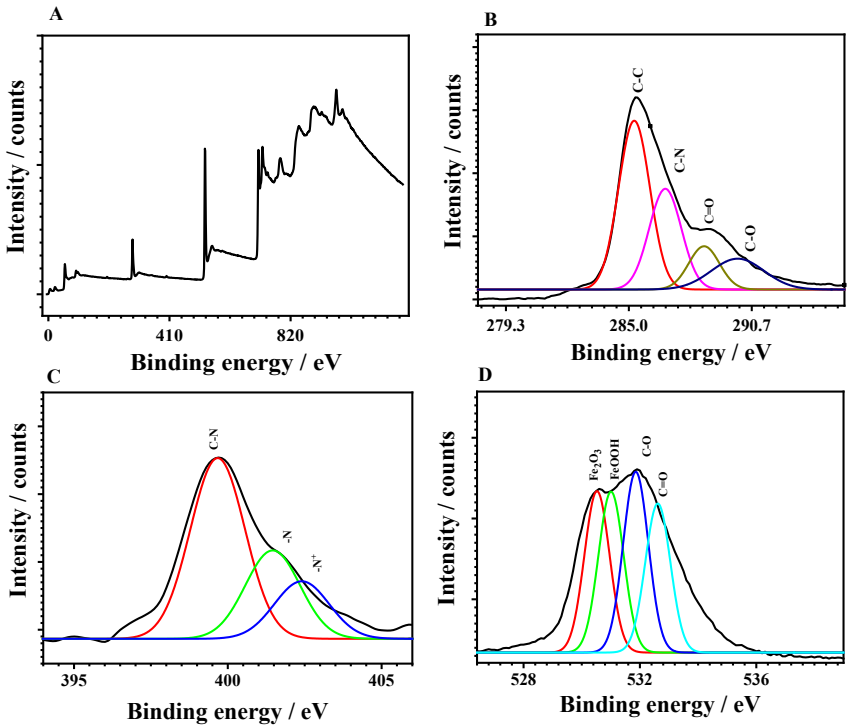

Fig. 10. (a) XPS survey scan composition of the API X120 steel immersed in the corrosion inhibitor and the profiles of (b) C 1s, (c) O 1s, and N 1s after 24 h immersion in 1 M H_2SO_4.

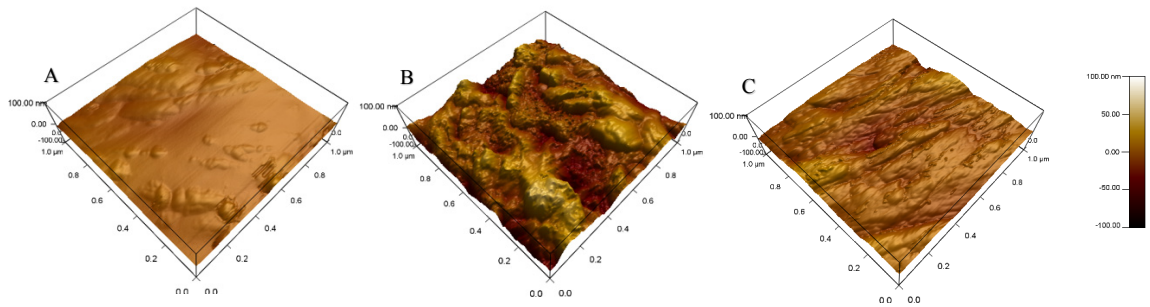

Fig. 11. AFM images for API X120 steel immersed in 1 M H_2SO_4 for 24 h in the absence and presence of 100 µmol L^{-1} of the CAPB at 20 °C

Theoretical studies of surfactant

The inhibition behavior of the investigated surfactant for API X120 steel corrosion in acidic solution could be discussed by quantum chemical studies. The optimized geometry, frontier molecular orbital of highest occupied molecular orbital (HOM, lowest unoccupied molecular orbital (LUMO), and the distribution of Mulliken charge of surfactant are diagrammed in Fig. 12. It is seen that; the distribution of electron densities were localized on HOMO and LUMO of surfactant which confirms the electron donating and accepting centers are possible in surfactant molecule. The detailed data of the quantum chemical parameters for surfactant is calculated and are listed in Table 7. The inhibition efficiency of investigated inhibitor for API X120 steel corrosion in acidic solution is related to the energy of lowest unoccupied molecular orbital (E_{LUMO}), the energy of highest occupied molecular orbital (E_{HOMO}) and the energy gap ΔE ($\Delta E = E_{LUMO} - E_{HOMO}$) [61]. From the Table 7, it can be noted that, the negative EHOMO values indicate that the surfactant molecule can easily give electrons to the empty d-orbital of iron. But, the lower E_{LUMO} values showed a higher electron accepting ability of the API X120 metal. The smaller values of ΔE showed the stability of forming complex on the API X120 steel surface [60]. Table 7 shows that the surfactant has the smallest *ΔE* paralleled with the HOMO and LUMO electronic density distributions of this molecule. Fig. 12 shows the HOMO of the studied compound that the N and O have a great electron density. .

Inhibitor	**Surfactant**
Mulliken Charges	
HOMO	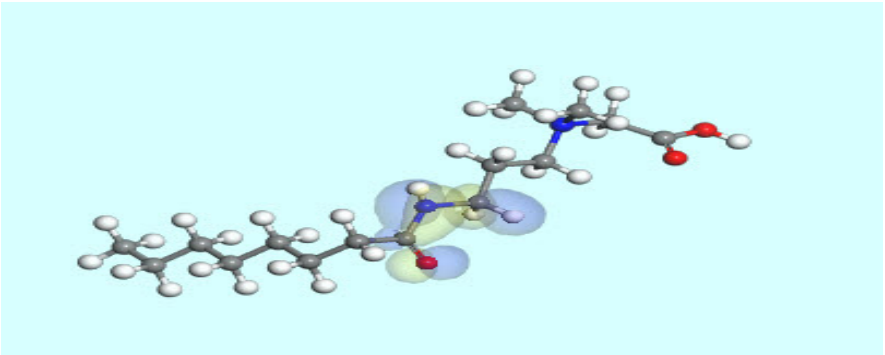
LUMO	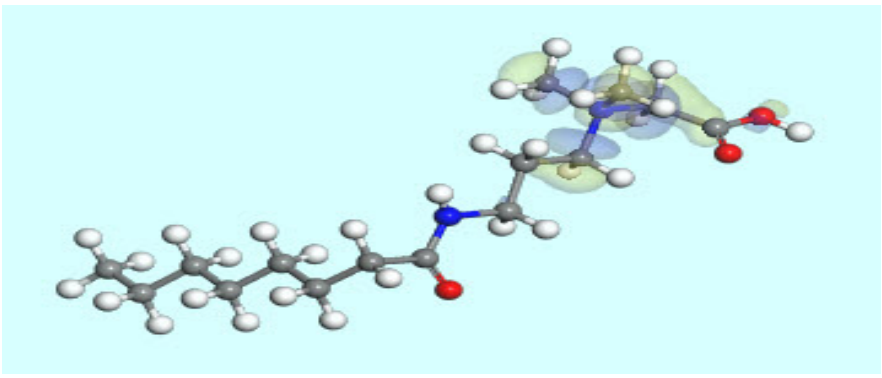

Fig. 12. The frontier molecular orbital examined surfactant (HOMO and LUMO).

TABLE 7. Parameter gotten from quantum for examining surfactant.

Parameter	E_{HOMO} (eV)	E_{LUMO} (eV)	ΔE (eV)	η (eV)	σ (eV^{-1})	Pi (eV)	χ (eV)	μ (debyes)
CAPB	-10.086	-0.477	9.609	4.805	0.208	-5.282	5.282	1.350

Mechanism of corrosion inhibition

The effectiveness of a corrosion inhibitor depends on the chemical structure of the organic compound. It is apparent from the chemical structure; this compound is able to adsorb on the metal surface via lone pair of electrons of N and O atoms. The Quaternary nitrogen atom (N^+) is adsorbed on the cathodic sites and decreases the evolution of hydrogen, also O atoms are adsorbed on the anodic sites and decrease the Fe dissolution. The high performance of inhibitor was attributed to the presence of adsorption centers, larger molecular size and the planarity of compound [61]. Figure 13 shows the scheme of the CAPB orientation on the API X120 surface in acidic medium, hemi micelle formation of inhibitor adsorbed on the API X120 surface at some sites of the surface leading to high inhibition efficiency resulting to large area covered by inhibitor. The hydrophobic chain may be oriented towards the aqueous medium and may also be arranged horizontally to the steel surface while hydrophilic chain is adsorbed on the steel surface [61]. This behavior is attributed to the saturation of the surface with surfactant molecules and the formation of multilayer.

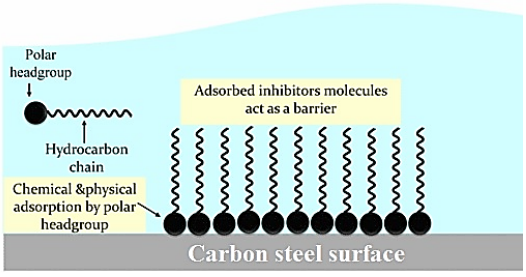

Fig. 13. Illustration of adsorption of surfactant on the API X120 surface

Summary and Conclusions

The CAPB green corrosion inhibitor has shown unusual performance at normal and elevated temperatures in inhibiting the corrosion of API X120 steel in 1 M H_2SO_4. The efficiency was found to increase as the inhibitor dose increased. When the testing temperature increased to 50 °C, a slight decline in efficiency was noted, due to the increased rate of iron dissolution in the acidic solution and the expected desorption of the adsorbed inhibitor from the metallic substrate. An IE of more than 94% was successfully achieved upon the addition of the inhibitor to a dose of 100 μmol L^{-1}. The relationship between the surface coverage and inhibitor dose is consistent with Langmuir's adsorption isotherm. The inhibitor is found to be of the mixed type. The adsorption of the inhibitor on the steel surface was proven to affect both cathodic and anodic reactions, which is confirmed by the calculated standard Gibbs free energy (ΔG^0_{ads}) and the energetic parameters from the quantum calculations. AFM analyses revealed a significant decrease in the surface roughness under an inhibited condition compared to immersion with no inhibitor added. Additionally, XPS revealed the presence of nitrogen on the API X120 steel, which validates the adsorption of the corrosion inhibitor molecules onto the surface. Applications of this inhibitor for the mitigation of acidic corrosion in the oil and gas industry will add value in terms of enabling safer operations and contributing to significant cost savings.

Acknowledgements

The findings achieved herein are solely the responsibility of the authors. Additionally, the authors thank the Center for Advanced Materials at Qatar University for their support.

Conflicts of Interest

The authors declare that there is no conflict of interest.

References

1. Zhang, K., Yang, W., Yin, X., Chen, Y., Liu, Y., Le, J., Xu, B. Amino acids modified konjac glucomannan as green corrosion inhibitors for mild steel in HCl solution. *Carbohydrate Polymers* **181** (Supplement C), 191-199 (2018), DOI: https://doi.org/10.1016/j.carbpol.2017.10.069.

2. Alvarez, P. E., Fiori-Bimbi, M. V., Neske, A., Brandán, S. A., Gervasi, C. A. *Rollinia occidentalis* extract as green corrosion inhibitor for carbon steel in HCl solution. *Journal of Industrial and Engineering Chemistry,* **58** (Supplement C), 92-99 (2018), DOI: https://doi.org/10.1016/j.jiec.2017.09.012.

3. Mobin, M., Rizvi, M. Polysaccharide from Plantago as a green corrosion inhibitor for carbon steel in 1M HCl solution. *Carbohydrate Polymers* **160** (Supplement C), 172-183 (2017), DOI: https://doi.org/10.1016/j.carbpol.2016.12.056.

4. Bello, M., Ochoa, N., Balsamo, V., López-Carrasquero, F., Coll, S., Monsalve, A., González, G. Modified cassava starches as corrosion inhibitors of carbon steel: An electrochemical and morphological approach. *Carbohydrate Polymers***, 82**(3), 561-568 (2010), DOI: https://doi.org/10.1016/j.carbpol.2010.05.019.

5. Mansfeld, F. Use of electrochemical impedance spectroscopy for the study of corrosion protection by polymer coatings. *Journal of Applied Electrochemistry*, **25**(3), 187-202 (**1995)**. DOI: 10.1007/bf00262955.

6. Obot, I. B., Ankah, N. K., Sorour, A. A., Gasem, Z. M., Haruna, K. 8-Hydroxyquinoline as an alternative green and sustainable acidizing oilfield corrosion inhibitor. *Sustainable Materials and Technologies,* **14** (Supplement C), 1-10 (2017). DOI: https://doi.org/10.1016/j.susmat.2017.09.001.

7. Kahyarian, A., Schumaker, A., Brown, B., Nesic, S. Acidic corrosion of mild steel in the presence of acetic acid: Mechanism and prediction. *Electrochimica Acta,* **258,** 639-652 (2017). DOI: https://doi.org/10.1016/j.electacta.2017.11.109.

8. Meriem-Benziane, M., Bou-Saïd, B., Boudouani, N. The effect of crude oil in the pipeline corrosion by the naphthenic acid and the sulfur: A numerical approach. *Journal of Petroleum Science and Engineering,* **158** (Supplement C), 672-679 (2017). DOI: https://doi.org/10.1016/j.petrol.2017.08.073.

9. Jin, P., Nesic, S. Mechanism of magnetite formation in high temperature naphthenic acid corrosion by crude oil fractions. *Corrosion Science,* **115** (Supplement C), 93-105 (2017). DOI: https://doi.org/10.1016/j.corsci.2016.11.021.

10. Olajire, A. A. Corrosion inhibition of offshore oil and gas production facilities using organic compound inhibitors - A review. *Journal of Molecular Liquids,* **248** (Supplement C), 775-808 (2017). DOI: https://doi.org/10.1016/j.molliq.2017.10.097.

11. Al Hashem, A. Corrosion in the Gulf Cooperation Council (GCC states: Statistics and figures. *Presented at the Corrosion UAE, Abu Dhabi, UAE* (2011).

12. Kaskah, S. E., Pfeiffer, M., Klock, H., Bergen, H., Ehrenhaft, G., Ferreira, P., Gollnick, J., Fischer, C. B. Surface protection of low carbon steel with N-acyl sarcosine derivatives as green corrosion inhibitors. *Surfaces and Interfaces,* **9** (Supplement C), 70-78 (2017). DOI: https://doi.org/10.1016/j.surfin.2017.08.002.

13. Parthipan, P., Narenkumar, J., Elumalai, P., Preethi, P. S., Usha Raja Nanthini, A., Agrawal, A., Rajasekar, A. Neem extract as a green inhibitor for microbiologically influenced corrosion of carbon steel API 5LX in a hypersaline environments. *Journal of Molecular Liquids,* **240** (Supplement C), 121-127 (2017). DOI: https://doi.org/10.1016/j.molliq.2017.05.059.

14. El-Hajjaji, F., Messali, M., Aljuhani, A., Aouad, M. R., Hammouti, B., Belghiti, M. E., Chauhan, D. S., Quraishi, M. A. Pyridazinium-based ionic liquids as novel and green corrosion inhibitors of carbon steel in acid medium: Electrochemical and molecular dynamics simulation studies. *Journal of Molecular Liquids,* **249** (Supplement C), 997-1008 (2018). DOI: https://doi.org/10.1016/j.molliq.2017.11.111.

15. Boumhara, K., Tabyaoui, M., Jama, C., Bentiss, F. *Artemisia mesatlantica* essential oil as green inhibitor for carbon steel corrosion in 1M HCl solution: Electrochemical and XPS investigations. *Journal of Industrial and Engineering Chemistry* **29** (Supplement C), 146-155 (2015). DOI: https://doi.org/10.1016/j.jiec.2015.03.028.

16. Feng, Y., Cheng, Y. F. An intelligent coating doped with inhibitor-encapsulated nanocontainers for corrosion protection of pipeline steel. *Chemical Engineering Journal,* **315** (Supplement C), 537-551 (2015). DOI: https://doi.org/10.1016/j.cej.2017.01.064.

17. Umoren, S. A., Obot, I. B., Madhankumar, A., Gasem, Z. M. Performance evaluation of pectin as ecofriendly corrosion inhibitor for X60 pipeline steel in acid medium: Experimental and theoretical approaches. *Carbohydrate Polymers* **124** (Supplement C), 280-291 (2015). DOI: https://doi.org/10.1016/j.carbpol.2015.02.036.

18. Bahgat Radwan, A., Sliem, M. H., Okonkwo, P. C., Shibl, M. F., Abdullah, A. M. Corrosion inhibition of API X120 steel in a highly aggressive medium using stearamidopropyl dimethylamine. *Journal of Molecular Liquids,* **236**, 220-231 (2015). DOI: https://doi.org/10.1016/j.molliq.2017.03.116.

19. Sliem, M. H., Afifi, M., Bahgat Radwan, A., Fayyad, E. M., Shibl, M. F., Heakal, F. E.-T., Abdullah, A. M. AEO7 Surfactant as an Eco-Friendly Corrosion Inhibitor for Carbon Steel in HCl solution. *Scientific Reports,* **9**(1), 2319 (2019). DOI: 10.1038/s41598-018-37254-7.

20. Worthen, A. J., Foster, L. M., Dong, J., Bollinger, J. A., Peterman, A. H., Pastora, L. E., Bryant, S. L., Truskett, T. M., Bielawski, C. W., Johnston, K. P. Synergistic Formation and Stabilization of Oil-in-Water Emulsions by a Weakly Interacting Mixture of Zwitterionic Surfactant and Silica Nanoparticles. *Langmuir,* **30**(4), 984-994 (2014). DOI: 10.1021/la404132p.

21. Worthen, A. J., Bryant, S. L., Huh, C., Johnston, K. P. Carbon dioxide-in-water foams stabilized with nanoparticles and surfactant acting in synergy. *AIChE Journal,* **59**(9), 3490-3501 (2013). DOI: 10.1002/aic.14124.

22. ASTM G 1-90, Standard practice for preparing, cleaning, and evaluating corrosion test specimens (1999).

23. Fontana, M. G. *Corrosion engineering*, Tata McGraw-Hill Education: (2006).

24. Raghavendra, N., Ishwara Bhat, J. Inhibition of Al corrosion in 0.5MHCl solution by Areca flower extract. *Journal of King Saud University - Engineering Sciences,* **31**(3), 202-208 (2019). DOI: https://doi.org/10.1016/j.jksues.2017.06.003.

25. Aloui, S., Sfaira, I. F., M., Ebn Touhami, M., Taleb, M., Filali Baba, M., Daoudi, M. New mechanism synthesis of 1,4-benzothiazine and its inhibition performance on mild steel in hydrochloric acid. *Port. Electrochim. Acta,* 27, 599-613 (2009).

26. Foad El-Sherbini, E. E., Deyab, S. M. A. W. M. Ethoxylated fatty acids as inhibitors for the corrosion of zinc in acid media. *Materials Chemistry and Physics,* **89**, 183-191 (2005).

27. Abdel Hameed, R. S. I., Omar M., Eissa, Fayez M., Ghanem, Raed. New non ionic polymeric surfactants as corrosion inhibitors for the C-steel alloy in hydrochloric acid corrosive medium. *Chemica Sinica,* **3**, 236-248 (2005).

28. Abdallah, M. Ethoxylated fatty alcohols as corrosion inhibitors for dissolution of zinc in hydrochloric acid. *Corrosion Science,* 45, 2705-2716 (2005).

29. Zeino, A., Abdulazeez, I., Khaled, M., Jawich, M. W., Obot, I. B. Mechanistic study of polyaspartic acid (PASP) as eco-friendly corrosion inhibitor on mild steel in 3% NaCl aerated solution. *Journal of Molecular Liquids,* **250**, 50-62 (2018). DOI: https://doi.org/10.1016/j.molliq.2017.11.160.

30. Guo, L., Kaya, S., Obot, I. B., Zheng, X., Qiang, Y. Toward understanding the anticorrosive mechanism of some thiourea derivatives for carbon steel corrosion: A combined DFT and molecular dynamics investigation. *Journal of Colloid and Interface Science,* **506** (Supplement C), 478-485 (2017). DOI: https://doi.org/10.1016/j.jcis.2017.07.082.

31. El-Sayed Shehata, O. Effect of acetamide derivative and its Mn-complex as corrosion inhibitor for mild steel in sulphuric acid. *Egyptian Journal of Chemistry,* **60**(2), 243-259 (2017). DOI: 10.21608/ejchem.2017.674.1014.

32. Peme, T., Olasunkanmi, O. L., Bahadur, I., Adekunle, S. A.; Kabanda, M. M., Ebenso, E. E. Adsorption and corrosion inhibition studies of some selected dyes as corrosion inhibitors for mild steel in acidic medium: gravimetric, electrochemical, quantum chemical studies and synergistic effect with iodide ions. *Molecules,* **20** (9) (2015). DOI: 10.3390/molecules200916004.

33. Chauhan, D. S., Ansari, K. R., Sorour, A. A., Quraishi, M. A., Lgaz, H., Salghi, R. Thiosemicarbazide and thiocarbohydrazide functionalized chitosan as ecofriendly corrosion inhibitors for carbon steel in hydrochloric acid solution. *International Journal of Biological Macromolecules,* (2017). DOI: https://doi.org/10.1016/j.ijbiomac.2017.10.050.

34. Salhi, A., Tighadouini, S., El-Massaoudi, M., Elbelghiti, M., Bouyanzer, A., Radi, S., El Barkany, S., Bentiss, F., Zarrouk, A. Keto-enol heterocycles as new compounds of corrosion inhibitors for carbon steel in 1M HCl: Weight loss, electrochemical and quantum chemical investigation. *Journal of Molecular Liquids,* **248** (Supplement C), 340-349 (2017). DOI: https://doi.org/10.1016/j.molliq.2017.10.040.

35. Bahgat Radwan, A., Sliem, M. H., Okonkwo, P. C., Shibl, M. F., Abdullah, A. M. Corrosion inhibition of API X120 steel in a highly aggressive medium using stearamidopropyl dimethylamine. *Journal of Molecular Liquids,* **236** (Supplement C), 220-231 (2017). DOI: https://doi.org/10.1016/j.molliq.2017.03.116.

36. Huttunen-Saarivirta, E., Rajala, P., Bomberg,

M., Carpén, L. EIS study on aerobic corrosion of copper in ground water: influence of micro-organisms. *Electrochimica Acta,* **240** (Supplement C), 163-174 (2017). DOI: https://doi.org/10.1016/j.electacta.2017.04.073.

37. Arabzadeh, H., Shahidi, M., Foroughi, M. M. Electrodeposited polypyrrole coatings on mild steel: Modeling the EIS data with a new equivalent circuit and the influence of scan rate and cycle number on the corrosion protection. *Journal of Electroanalytical Chemistry,* **807** (Supplement C), 162-173 (2017). DOI: https://doi.org/10.1016/j.jelechem.2017.11.019.

38. Li, J., Ecco, L., Fedel, M., Ermini, V., Delmas, G., Pan, J. In-situ AFM and EIS study of a solventborne alkyd coating with nanoclay for corrosion protection of carbon steel. *Progress in Organic Coatings,* **87** (Supplement C), 179-188 (2015). DOI: https://doi.org/10.1016/j.porgcoat.2015.06.003.

39. El jaouhari, A., Kaya, S., Ben jadi, S., Aouzal, Z., Bouabdellaoui, M., Bazzaoui, E. A., Erdoğan, Ş., Bazzaoui, M. Experimental and MDS studies of corrosion inhibition of carbon steel by saccharinate sodium. *Surfaces and Interfaces* **10** (Supplement C), 11-18 (2018). DOI: https://doi.org/10.1016/j.surfin.2017.11.003.

40. Abd El Wanees, S., Bahgat Radwan, A., Alsharif, M. A., Abd El Haleem, S. M. Initiation and inhibition of pitting corrosion on reinforcing steel under natural corrosion conditions. *Materials Chemistry and Physics,* **190** (Supplement C), 79-95 (2017). DOI: https://doi.org/10.1016/j.matchemphys.2016.12.048.

41. Fouda, A. S., Killa, H. M., Farouk, A., Salem, A. M. Calicotome extract as a friendly corrosion inhibitor for carbon steel in polluted NaCl solution: chemical and electrochemical studies. *Egyptian Journal of Chemistry,* **62**(10), 1879-1894 (2019). DOI: 10.21608/ejchem.2019.7656.1649.

42. Obot, I. B.; Onyeachu, I. B.; Kumar, A. M. Sodium alginate: A promising biopolymer for corrosion protection of API X60 high strength carbon steel in saline medium. *Carbohydrate Polymers* **2017,** *178* (Supplement C), 200-208, DOI: https://doi.org/10.1016/j.carbpol.2017.09.049.

43. Machuca, L. L., Lepkova, K., Petroski, A. Corrosion of carbon steel in the presence of oilfield deposit and thiosulphate-reducing bacteria in CO2 environment. *Corrosion Science,* **129** (Supplement C), 16-25 (2017). DOI: https://doi.org/10.1016/j.corsci.2017.09.011.

44. Fouda, A. S., Ismail, M. A., Al-Khamri, A. A., Abousalem, A. S. Experimental, quantum chemical and molecular simulation studies on the action of arylthiophene derivatives as acid corrosion inhibitors. *Journal of Molecular Liquids,* **290**, 111178 (2019). DOI: https://doi.org/10.1016/j.molliq.2019.111178.

45. Fouda, A. S., Ismail, M. A., Temraz, A. M., Abousalem, A. S. Comprehensive investigations on the action of cationic terthiophene and bithiophene as corrosion inhibitors: experimental and theoretical studies. *New Journal of Chemistry,* **43**(2), 768-789 (2019). DOI: 10.1039/C8NJ04330B.

46. Liu, X., Cheng, Y., Wang, W., Liu, F., Hou, B. Application of 1D attapulgite as reservoir with benzotriazole for corrosion protection of carbon steel. *Materials Chemistry and Physics,* **205** (Supplement C), 292-302 (2018). DOI: https://doi.org/10.1016/j.matchemphys.2017.11.038.

47. El Wanees, S. A., Alahmdi, M. I., Alsharif, M. A., Atef, Y. Mitigation of hydrogen evolution during zinc corrosion in aqueous acidic media using 5-Amino-4-imidazolecarboxamide. *Egyptian Journal of Chemistry,* **62**(5), 1211-1225 (2019). DOI: 10.21608/ejchem.2018.6006.1507.

48. Abdelaal, M. M., Mohamed, S., Barakat, Y. F., Derbala, H. A. Y., Hassan, H. H., Al Zoubi, W. N-Aminophthalimide as a synthon for heterocyclic Schiff bases: efficient utilization as corrosion inhibitors of mild steel in 0.5 mol.L-1 H2SO4 solution. *Egyptian Journal of Chemistry,* **61**(3), 539-558 (2018). DOI: 10.21608/ejchem.2018.2414.1198.

49. Almzarzie, K., Falah, A., Massri, A., Kellawi, H. Electrochemical impedance spectroscopy (EIS) and study of iron corrosion inhibition by turmeric roots extract (TRE) in hydrochloric acid solution. *Egyptian Journal of Chemistry,* **62**(3), 501-512 (2019). DOI: 10.21608/ejchem.2018.5295.1476.

50. Kannan, P., Rao, T. S., Rajendran, N. improvement in the corrosion resistance of carbon steel in acidic condition using naphthalen-2-ylnaphthalene-2-carboxammide inhibitor. *Journal of Colloid and Interface Science,* **512** (Supplement C), 618-628 (2018). DOI: https://doi.org/10.1016/j.jcis.2017.09.061.

51. Kaczerewska, O., Leiva-Garcia, R., Akid,

R., Brycki, B., Kowalczyk, I., Pospieszny, T. Effectiveness of O-bridged cationic gemini surfactants as corrosion inhibitors for stainless steel in 3 M HCl: experimental and theoretical studies. *Journal of Molecular Liquids,* **249**, 1113-1124 (2018). DOI: https://doi.org/10.1016/j.molliq.2017.11.142.

52. Lgaz, H., Salghi, R., Subrahmanya Bhat, K., Chaouiki, A., Shubhalaxmi, Jodeh, S. Correlated experimental and theoretical study on inhibition behavior of novel quinoline derivatives for the corrosion of mild steel in hydrochloric acid solution. *Journal of Molecular Liquids,* **244**, 154-168 (2017). DOI: https://doi.org/10.1016/j.molliq.2017.08.121.

53. Bouanis, M., Tourabi, M., Nyassi, A., Zarrouk, A., Jama, C., Bentiss, F. Corrosion inhibition performance of 2,5-bis(4-dimethylaminophenyl)-1,3,4-oxadiazole for carbon steel in HCl solution: Gravimetric, electrochemical and XPS studies. *Applied Surface Science,* **389** (Supplement C), 952-966 (2016). DOI: https://doi.org/10.1016/j.apsusc.2016.07.115.

54. El Hamdani, N., Fdil, R., Tourabi, M., Jama, C., Bentiss, F. Alkaloids extract of *Retama monosperma* (L.) Boiss. seeds used as novel eco-friendly inhibitor for carbon steel corrosion in 1M HCl solution: Electrochemical and surface studies. *Applied Surface Science,* **357** (Part A), 1294-1305 (2015). DOI: https://doi.org/10.1016/j.apsusc.2015.09.159.

55. Azzaoui, K., Mejdoubi, E., Jodeh, S., Lamhamdi, A., Rodriguez-Castellón, E.,Algarra, M., Zarrouk, A., Errich, A., Salghi, R., Lgaz, H. Eco friendly green inhibitor Gum Arabic (GA) for the corrosion control of mild steel in hydrochloric acid medium. *Corrosion Science,* **129** (Supplement C), 70-81 (2017). DOI: https://doi.org/10.1016/j.corsci.2017.09.027.

56. Outirite, M., Lagrenée, M., Lebrini, M., Traisnel, M., Jama, C., Vezin, H., Bentiss, F. Ac impedance, X-ray photoelectron spectroscopy and density functional theory studies of 3,5-bis(n-pyridyl)-1,2,4-oxadiazoles as efficient corrosion inhibitors for carbon steel surface in hydrochloric acid solution. *Electrochimica Acta,* **55**(5), 1670-1681 (2010). DOI: https://doi.org/10.1016/j.electacta.2009.10.048.

57. Zhang, Z., Tian, N., Zhang, L., Wu, L. Inhibition of the corrosion of carbon steel in HCl solution by methionine and its derivatives. *Corrosion Science,* **98** (Supplement C), 438-449 (2015). DOI: https://doi.org/10.1016/j.corsci.2015.05.048.

58. Singh, P., Srivastava, V., Quraishi, M. A. Novel quinoline derivatives as green corrosion inhibitors for mild steel in acidic medium: Electrochemical, SEM, AFM, and XPS studies. *Journal of Molecular Liquids,* **216** (Supplement C), 164-173 (2016). DOI: https://doi.org/10.1016/j.molliq.2015.12.086.

59. Ouici, H., Tourabi, M., Benali, O., Selles, C., Jama, C., Zarrouk, A., Bentiss, F. Adsorption and corrosion inhibition properties of 5-amino 1,3,4-thiadiazole-2-thiol on the mild steel in hydrochloric acid medium: thermodynamic, surface and electrochemical studies. *Journal of Electroanalytical Chemistry,* **803** (Supplement C), 125-134 (2017). DOI: https://doi.org/10.1016/j.jelechem.2017.09.018.

60. Yadav, M., Sarkar, T. K., Obot, I. B. Carbohydrate compounds as green corrosion inhibitors: electrochemical, XPS, DFT and molecular dynamics simulation studies. *RSC Advances,* **6** (111), 110053-110069 (2016). DOI: 10.1039/c6ra24026g.

61. Migahed, M. A., Elgendy, A., El-Rabiei, M. M., Nady, H., Zaki, E. G. Novel Gemini cationic surfactants as anti-corrosion for X-65 steel dissolution in oilfield produced water under sweet conditions: Combined experimental and computational investigations. *Journal of Molecular Structure,* **1159,** 10-22 (2018). DOI: https://doi.org/10.1016/j.molstruc.2018.01.033.

كابروراميدوبروبايل بيتان كأحد مثبطات التآكل الصديقة للبيئة وذات الكفاءة العالية للصلب API X120في 1 مولر حمض الكبريتيك

عبد العزيز فودة[١]، على عبد العال[٢]، مصطفى سليم[٢]، أبو بكر محمد عبد الله[٣]
[١] قسم الكيمياء - كلية العلوم - جامعة المنصورة - المنصورة - مصر.
[٢] قسم الكيمياء - كلية العلوم - جامعة الزقازيق - الزقازيق - مصر.
[٣] مركز المواد المتقدمة ، جامعة قطر - الدوحة - قطر.

تم دراسة تثبيط تآكل الصلب API X120 في محلول 1 مولر حمض الكبريتيك في درجات حرارة متغيرة باستخدام المركب الجديد الصديق للبيئة (كابروراميدوبروبايل بيتان (كابب))عن طريق اختبار الوزن والكهروكيميائية (التي تحتوي على الجهد الكهربي الاستقطابى و مطيافية الممانعه الكهروكيميائية). يتم استخدام اختبارات توصيف السطح التي تحتوي على الماسح المجهري للإلكترون (SEM) ومجهر القوة الذرية (AFM) في الدراسة ، بالإضافة إلى ذلك، تم قياس ومناقشة المعلمات الحركية والديناميكية الحرارية ، وأظهرت النتائج الإجمالية أن معدل التآكل في الصلب API X120 تم خفضه بشكل كبير مع زيادة درجة الحرارة. تؤثر منحنيات الاستقطاب المؤدية إلى المثبط كابب على كل من التفاعلات الأنوديه والكاثوديه (مثبط من النوع المختلط) وقد حددت تحليلات طبوغرافيا السطح انخفاضًا ملموسًا في خشونة السطح مع زيادة جرعة المثبط في المحلول، الأشعة السينية والأشعة السينية الضوئية المشتتة للطاقة كشفت عن وجود ذرات نيتروجين ممتزه على اسطح الصلب API X 120 . يوفر هذا العمل مثبطًا واعداً صديقًا للبيئة لتقليل تآكل الصلب API X120 في بيئات شديدة الحمضية.